Макрогетероциклы
http://macroheterocycles.isuct.ru

DOI: 10.6060/mhc210338p

A Covalently Linked Dyad Based on Zinc Phthalocyanine and Methylpheophorbide *a*: Synthetic and Physicochemical Study

Irina O. Balashova,[a] Alexander Yu. Tolbin,[a] Pavel A. Tarakanov,[a] Alexei R. Krot,[b] Kseniya V. Fedorova,[b] Irina A. Sergeeva,[b] Stanislav A. Trashin,[a,c] Karolien De Wael,[c] Victor E. Pushkarev,[a@] Mikhail O. Koifman,[d] and Gelii V. Ponomarev[e]

[a]*Institute of Physiologically Active Compounds, Russian Academy of Sciences, 142432 Chernogolovka, Moscow Region, Russia*
[b]*Department of Physics, M.V. Lomonosov Moscow State University, 119991 Moscow, Russia*
[c]*AXES Research Group, Department of Chemistry, University of Antwerp, 2020 Antwerpen, Belgium*
[d]*Ivanovo State University of Chemistry and Technology, Research Institute of Macroheterocycles, 153000 Ivanovo, Russia*
[e]*V.N. Orekhovich Institute of Biomedical Chemistry, 119121 Moscow, Russia*
[@]*Corresponding author E-mail: pushkarev@ipac.ac.ru*

Dedicated to the memory of Professor Larisa G. Tomilova

The first covalently linked conjugate of metal phthalocyaninate and chlorin e_6 derivative has been obtained by transesterification of α-ketomethyl ester in methylpheophorbide a with zinc(II) 2-(2-hydroxymethylbenzyloxy)-9(10),16(17),23(24)-tri-tert-butylphthalocyaninate under mild conditions. The dyad exhibits a panchromatic nature revealing both the phthalocyanine and pheophorbide derived bands in the UV-Vis absorption spectrum. The ^{1}H NMR spectroscopy data combined with theoretical calculations indicate the presence of spatial intramolecular interactions between the phthalocyanine, pheophorbide and spacer fragments of the dyad allowing to forecast its enhanced nonlinear optical properties, as well as the characteristic energy transfer from the excited pheophorbide subunit to the phthalocyanine core. Indeed, when excited in the UV-Vis range, the conjugate shows red fluorescence with the spectral maximum at 686 nm, which is close to the one of the initial zinc phthalocyaninate. Furthermore, the dyad effectively generates singlet oxygen and, in the presence of polyvinylpyrrolidone (PVP) as biocompatible solubilizer, forms stable micellar saline solutions with the particles ranged in size between 40 and 100 nm. These nanoparticles represent promising third-generation photosensitizing systems for application in theranostics.

Keywords: Phthalocyanine, methylpheophorbide *a*, transesterification, panchromatic absorption, fluorescence, singlet oxygen generation, micellar nanoparticles, dynamic light scattering.

Ковалентно связанная диада на основе фталоцианина цинка и метилфеофорбида *a*: синтез и физико−химические исследования

И. О. Балашова,[a] А. Ю. Толбин,[a] П. А. Тараканов,[a] А. Р. Крот,[b] К. В. Федорова,[b] И. А. Сергеева,[b] С. А. Трашин,[a,c] К. Де Ваэль,[c] В. Е. Пушкарев,[a@] М. О. Койфман,[d] Г. В. Пономарев[e]

[a]*Институт физиологически активных веществ РАН, 142432 Черноголовка, Россия*
[b]*Московский государственный университет имени М.В. Ломоносова, Физический факультет, 119991 Москва, Россия*
[c]*Исследовательская группа AXES, Университет Антверпена, Химический факультет, 2020 Антверпен, Бельгия*
[d]*Институт макрогетероциклических соединений, Ивановский государственный химико-технологический*

университет, 153000 Иваново, Россия
[c]*Институт биомедицинской химии имени В.Н. Ореховича, 119121 Москва, Россия*
[@]*E-mail: pushkarev@ipac.ac.ru*

Посвящается памяти профессора Ларисы Годвиговны Томиловой

Впервые синтезирован ковалентный конъюгат на основе металлофталоцианина и производного хлорина e_6 путем переэтерификации α-кетометилового эфирного фрагмента метилфеофорбида а 2-(2-гидроксиметилбензилокси)-9(10),16(17),23(24)-три-трет-бутилфталоцианинатом цинка(II) в мягких условиях. Диада проявляет панхроматическую природу, её ЭСП содержит характерные полосы фталоцианинового и феофорбидного хромофоров. Данные ^{1}H ЯМР спектроскопии в совокупности с теоретическими расчетами говорят о наличии пространственных внутримолекулярных взаимодействий между фталоцианиновым, феофорбидным и спейсерным фрагментами диады, позволяя прогнозировать выраженные нелинейно-оптические свойства, а также характерный перенос энергии от возбужденной субъединицы феофорбида к фталоцианиновому ядру. При возбуждении в видимом диапазоне конъюгат демонстрирует красную флуоресценцию с максимумом при 686 нм, близким к максимуму исходного фталоцианината цинка. Более того, диада эффективно генерирует синглетный кислород и в присутствии поливинилпирролидона (ПВП) в качестве биосовместимого солюбилизатора формирует в физиологическом растворе стабильные мицеллы размером от 40 до 100 нм. Данные наночастицы можно рассматривать в качестве перспективного фотосенсибилизатора третьего поколения для тераностики.

Ключевые слова: Фталоцианин, метилфеофорбид *a*, переэтерификация, панхроматическое поглощение, флуоресценция, генерация синглетного кислорода, мицеллярные наночастицы, динамическое светорассеяние.

Introduction

Phthalocyanine–porphyrin (Pc–Por) hetero-array systems owing to their unique composition show specific intramolecular interactions,[1-12] which result in efficient photo-induced electron and/or energy transfer processes from porphyrin to phthalocyanine macrocycle and typically strong fluorescence of the latter due to fluorescence resonance energy transfer (FRET) process.[11,12] This renders them good candidates for application in electrochemical catalysis,[13] light-harvesting[14,15] and optoelectronic devices.[16] By themselves, phthalocyanines and porphyrins, in particular, chlorin e_6 derivatives, are also known as quite efficient photosensitizers (PSs) used in photodynamic therapy (PDT) owing to the ability of the photo-induced singlet oxygen ($^1O_2$) generation.[17,18] Moreover, they can be readily applied in such a modern field as theranostics, which combines therapy and diagnosis of diseases.[19-22] With such a background, it is rather surprising that Pc–Por hetero-conjugates, to the best of our knowledge, have not yet been investigated as agents for PDT and theranostics. We tend to explain this by comparatively low synthetic availability of low-symmetry A_3B-type phthalocyanines, which constitute these conjugates. However, our recent research has allowed to increase the yields of these compounds up to 50 %[23] making them available for the further synthetic and applied studies.[24-38] In one of these studies,[32] we reported the first synthesis of a covalently linked dyad comprising Pc and methylpheophorbide *a* (Pheo) subunits. Since Pc metal complexes are known to be better PSs than the corresponding free-base ligands, herein, we extend the range of Pc–Pheo dyads by a derivative bearing a zinc(II) Pc (PcZn) subunit. Here we report on structural features and physico-chemical properties of the PcZn-Pheo dyad with a brief evaluation of its applied potential in non-linear optics and as a PDT/imaging agent for theranostics.

Experimental

Methylpheophorbide *a* (**1**) can be prepared by any of the known procedures.[39-41] Zinc(II) 2-(2-hydroxymethylbenzyloxy)-9(10),16(17),23(24)-tri-*tert*-butylphthalocyaninate (**2**) represents a mixture of regioisomers and can be synthesized following two alternative procedures.[24,42] 4-Dimethylaminopyridine (DMAP) was purchased from Aldrich. Polyvinylpyrrolidone PVP-K30 (PVP, $M_w \approx 44000–54000$) was purchased from PanReac AppliChem. All other reagents and solvents were obtained or distilled according to standard procedures. The reaction was TLC and UV-Vis controlled until complete disappearance of starting phthalocyanine compound **2**. Gel permeation chromatography was performed on the polymeric support Bio-Beads S-X1 (BIORAD) using toluene as the eluent. Preparative TLC was performed using Merck Silica Gel 60 flexible plates with toluene÷MeOH (10:1 vol.) mixture as the eluent. MALDI-TOF mass spectra were obtained using Bruker Autoflex II mass spectrometer with α-cyano-4-hydroxycinnamic acid (CHCA) as the matrix. 1D and 2D ^{1}H NMR spectra were registered on Bruker AM-200 (200 MHz) and Bruker Avance 500 (500 MHz) instruments using $CDCl_3$, DMSO-d_6 or DMF-d_7 as the solvent.

UV-Vis and fluorescence spectra were recorded on Hitachi U-2900 spectrophotometer and Varian Cary Eclipse fluorescence spectrophotometer, respectively, in toluene, DMF and/or THF using quartz cells (10×10 mm). The comparative method using a solution of fluorescein in 0.01 M KOH in 95 % ethanol as the standard was applied to determine the fluorescence quantum yields (Φ_f(fluorescein) = 0.97 with λ_{ex} = 470 nm).[43] The calculation of fluorescence quantum yield (Φ_f) was made according to the following equation:[44]

$$\Phi_f^S = \frac{G^S A_\lambda^R n_{toluene}^2}{G^R A_\lambda^S n_{ethanol}^2} \cdot \Phi_f^R ,$$

where G is the integrated emission area, n is the refractive index of the solvent, A_λ is the absorbance at the excited wavelength, and Φ_f is the fluorescence quantum yield. The indexes S and R correspond to the sample and the reference, respectively.

The singlet oxygen ($^1O_2$) quantum yields (Φ_Δ) were measured in freshly prepared solutions in toluene containing 56 μM

1,3-diphenylisobenzofuran (DPBF, Acros, 97 % purity) as a singlet oxygen quencher. The measurements were carried out in a 10 mm quartz cuvette under continuous stirring and illumination with a red LED laser (Roithner Lasertechnik, Austria) with λ_{laser} = 659 nm and an output power adjusted to 2 mW. Concentrations of the photosensitizers were adjusted in the range 5–10 μM to get absorbance close to 0.2 at λ_{laser}. UV-Vis absorption spectra were recorded automatically every 20 s using AvaSpec-2048L equipped with AvaLight-DH-S-BAL (Avantes BV, the Netherlands). The Φ_Δ values were determined by the comparison method using *meso*-tetraphenylporphyrin (TPP, Acros, 97 % purity) as the reference photosensitizer and calculated according to the equation:

$$\Phi_\Delta^S = \frac{S^{S_i R}}{S^{R_i S}} \cdot \Phi_\Delta^R ,$$

where S represents the slope for consumption of DPBF at 439 nm; $I = \Sigma_i I_0(\lambda_i) \times (I - 10^{-A(\lambda i)})$, where $I_0(\lambda_i)$ and $A(\lambda_i)$ are the laser radiation intensity and absorbance of the photosensitizer at a corresponding wavelength λ_i. The value of $\Phi_\Delta^R = 0.68 \pm 0.06$ for TPP[45] was used as the reference. All measurements were conducted in at least three repetitions.

Sonication of mixtures of dyad **3** and PVP in saline to obtain micellar solutions was performed using a Bandelin Sonopuls Ultrasonic Homogenizer HD 3100. Parameters for dispersions of nanoparticles in micellar solutions were measured using a Photocor-Complex optical setup equipped with a diode laser with λ = 647 nm and a power of 25 mW. The device is assembled as a dynamic light scattering (DLS) spectrometer designed for multi-angle DLS measurements and particle size measurements. The light beam hit the focusing unit and passed through the cuvette with the test solution; intensity of the light scattered at an angle of 90° (I) was recorded by a PerkinElmer avalanche photodiode. The temperature in the cuvette with the test sample was maintained at 20 °C using a built-in thermostat. A multichannel correlator (288 channels) was used, and the signal was processed on a PC in automatic mode using the DynaLS software, which allows obtaining results in the form of the translational diffusion coefficient (D_t) and hydrodynamic radius (R_h) values (*https://www.photocor.ru/*).

Density functional theory (DFT) calculations were performed using the quantum-chemical program PRIRODA[46] without solvent effects and symmetry constraints. The gradient-corrected exchange-correlation Perdew, Burke, and Ernzerhof (PBE) functional[47] as well as cc-pVDZ basis set[48] were used both for optimization of the structure geometries corresponded to steady-state and for scanning of the potential energy surfaces (PESs). The peripheral *tert*-butyl substituents on the phthalocyanine macrocycle were omitted to reduce the calculation time. The 10^{-6} threshold on the orbital gradients at the energy calculations tag and 10^{-4}–10^{-5} threshold on the molecular gradient at the geometry optimization procedure were employed. The valence shells were described by basis sets with the following contraction schemes: {6s2p}/[2s1p] on H; {10s7p3d}/[3s2p1d] on C, N, O; and {19s15p11d5f}/[6s5p3d1f] on Zn atom, respectively. The systematic vibrational analysis was performed to confirm whether an optimized geometry corresponds to a transition state (or a saddle point) with only one imaginary frequency or a minimum without an imaginary frequency. The construction of the 3D surface demonstrating the variation of the tilt and rotation angles towards the total energy of the system is performed using *Geometry Analyzer* Module for EasyQuanto.[49]

The structures corresponding to local minima obtained by scanning the PESs have been re-optimized on the B3LYP/6-31+G* level of theory using the GAMESS (US) software package.[50] *Ab initio* calculations of static polarizabilities (α), first (β) and second (γ) hyperpolarizabilities were carried out within the framework of the finite-field DFT method (FF-DFT, F = 0.001 a.u.) to evaluate the ability of the macroheterocyclic compounds to exhibit nonlinear optical (NLO) properties. All the quantum chemical calculations (gas-phase) were performed on an Intel/Linux cluster (Joint Supercomputer Center of Russian Academy of Sciences – *http://www.jscc.ru*). Visualization of the optimized structures was performed with the *Mercury* program obtained from the Cambridge Crystallographic Data Centre (*http://www.ccdc.cam.ac.uk*).

In this work, we first report the ^{1}H NMR spectrum of extra-pure compound **2** recorded in DMSO-d_6. The ^{1}H NMR, mass spectrometry, UV-Vis and fluorescence data for **1** and **2** are given below to facilitate evaluation of the corresponding data for target dyad **3**.

*Spectral data of compound **1**.* ^{1}H NMR ($CDCl_3$) δ_H ppm (J Hz): 9.29–9.34 (m, 1H, 10-H), 9.11–9.16 (m, 1H, 5-H), 8.49, 8.54 (2s, 1H, 20-H), 7.75–7.91 (dd, 1H, $^3J_{trans}$ = 17.8, $^3J_{cis}$ = 11.8, 3^1-H), 6.28 (s, 1H, 13^2-H), 6.14–6.23 (dd, 1H, $^3J_{trans}$ = 17.8, $^2J_{gem}$ = 1.8, *trans*-3^2-H), 6.06–6.13 (dd, 1H, $^3J_{cis}$ = 11.8, $^2J_{gem}$ = 1.8, *cis*-3^2-H), 4.42–4.53 (quartet, 1H, ^3J = 7.1, 18-H), 4.17–4.32 (m, 1H, 17-H), 3.87, 3.92 (2s, 3H, Me^2), 3.65 (s, 3H, 12^1-H), 3.61 (s, 3H, Me^1-H), 3.41–3.54 (m, 2H, 8^1-H), 3.33 (s, 3H, 2^1-H), 3.04 (s, 3H, 7^1-H), 2.47–2.75 (m, 2H, 17^2-H), 2.19–2.40 (m, 2H, 17^1-H), 1.85 (d, 3H, ^3J = 7.1, 18^1-H), 1.61 (t, 3H, ^3J = 7.3, 8^2-H), 0.45, –1.54, –1.75 (3 br s, 2H, N-H). UV-Vis (toluene) λ nm (I/I_{max}): 322 (0.21), 412 (1.00), 507 (0.10), 536 (0.09), 612 (0.07), 670 (0.48). UV-Vis (DMF) λ nm (I/I_{max}): 327 (0.24), 411 (1.00), 506 (0.11), 535 (0.10), 609 (0.08), 666 (0.42). UV-Vis (THF) λ nm (lg ε): 277 (4.28), 321 (4.40), 410 (5.02), 506 (4.12), 535 (4.05), 609 (3.96), 667 (4.68). Fluorescence (toluene) λ nm (λ_{ex} = 610 nm): 676.

*Spectral data of compound **2**.* ^{1}H NMR (DMSO-d_6) δ_H ppm: 9.27–9.38 (m, 3H, α′-H^{Ar,Pc}), 9.01–9.24 (m, 3H, α-H^{Ar,Pc}), 8.79–8.96 (m, 1H, α^1-H^{Ar,Pc}), 8.40–8.66 (m, 1H, α′^{1}-H^{Ar,Pc}), 8.19–8.31 (m, 3H, β-H^{Ar,Pc}), 7.63–7.89 (group m, 2H, α-H^{Ar,sp}), 7.56–7.60 (m, 1H, β^1-H^{Ar,Pc}), 7.43–7.53 (m, 2H, β-H^{Ar,sp}), 5.67–5.73 (m, 2H, 1-CH_2^{sp}), 5.41–5.45 (m, 1H, OH^{sp}), 4.92–4.97 (m, 2H, 2-CH_2^{sp}), 1.76–1.82 (group s, 27H, H-^{t}Bu^{Pc}). MALDI-TOF *m/z*: 880.32 $[M]^+$ (calculated for $C_{52}H_{48}N_8O_2Zn$: 880.32); 759.34 $[M–C_8H_9O]^+$ (calculated for $C_{44}H_{39}N_8OZn$: 759.25). UV-Vis (toluene) λ nm (I/I_{max}): 354 (0.47), 611 (0.20), 652sh (0.21), 677 (1.00). UV-Vis (DMF) λ nm (I/I_{max}): 351 (0.42), 610 (0.17), 647sh (0.19), 676 (1.00). Fluorescence (toluene) λ nm (λ_{ex} = 610 nm): 684.

*Preparation of dyad **3**.* A mixture of methylpheophorbide *a* **1** (15.2 mg, 0.025 mmol), phthalocyanine **2** (13.3 mg, 0.015 mmol), DMAP (1.8 mg, 0.015 mmol) and catalytic amount of I_2 dissolved in 5 ml of toluene was refluxed for 3 h. The solvent was removed *in vacuo*, then the mixture was reprecipitated from the MeOH÷H_2O (70:30 vol.) mixture leading to partial separation of the unreacted pheophorbide **1**. The solid residue was dissolved in toluene and purified by gel permeation chromatography to isolate the second blue-green band, which was dried *in vacuo* after evaporation of the solvent. Additional purification of the resulting solid by preparative TLC yielded a blue-green band of high-purity product **3** (11.8 mg, 54 %). R_f (toluene) = 0.65. MALDI-TOF *m/z*: 1454.68 $[M]^+$ (calculated for $C_{87}H_{82}N_{12}O_6Zn$: 1454.58); 880.41 $[M–C_{35}H_{35}N_4O_4+H]^+$ (calculated for $C_{52}H_{48}N_8O_2Zn$: 880.32); 759.48 $[M–C_{43}H_{43}N_4O_5]^+$ (calculated for $C_{44}H_{39}N_8OZn$: 759.25); 547.38 $[M–C_{53}H_{47}N_8O_3Zn]^+$ (calculated for $C_{34}H_{35}N_4O_3$: 547.27). ^{1}H NMR (DMF-d_7) δ_H ppm: 9.50–9.61 (m, 3H, α′-H^{Ar,Pc}), 9.33–9.45 (m, 3H, α-H^{Ar,Pc}), 9.33–9.61 (2m overlapped with α-H^{Ar,Pc} and α′-H^{Ar,Pc}, 2H, 5,10-H^{pheo}), 8.60–9.12 (group br m, 2H, α′^{1}-H^{Ar,Pc}, α^1-H^{Ar,Pc}), 8.28–8.40 (group br m, 4H, β-H^{Ar,Pc}, 20-H^{pheo}), 8.15–8.23 (br m, 1H, 3^1-H^{pheo}), 7.30–7.65 (group br m, 2H, α-H^{Ar,sp}), 7.10–7.49 (group m, 1H, β^1-H^{Ar}), 7.10–7.37 (group br m, 2H, β-H^{Ar,sp}), 5.96–6.50 (group br m, 2H, 3^2-H^{pheo}), 5.67–5.88 (group m, 3H, 1-CH_2^{sp}, 13^2-H^{pheo}), 5.18–5.44 (br m, 2H, 2-CH_2^{sp}), 4.47–4.64 (br m, 1H, 18-H^{pheo}), 4.32–4.41 (br m, 1H,† 17-H^{pheo}), 3.76–3.90 (br m, 2H,

†The observed integral value is lower due to H/D exchange interaction.

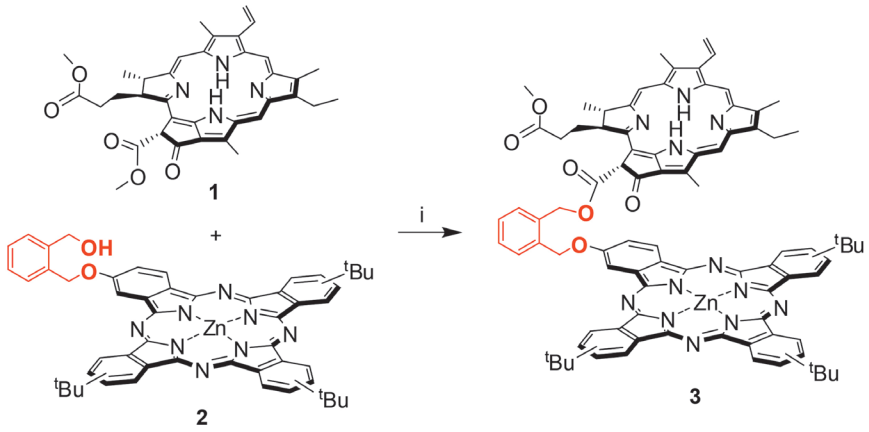

Scheme 1. Synthesis of dyad **3**. *i* = I_2, DMAP, toluene, 110 °C.

8^1-H^{pheo}), 3.42–3.70 (group s, 12H, H-MeO^{pheo}, 2^1-H^{pheo}, 7^1-H^{pheo}, 12^1-H^{pheo}), 2.95–3.08 (br m, 2H,‡ 17^2-H^{pheo}), 2.17–2.53 (group br m, 2H, 17^1-H^{pheo}), 1.79–1.89 (group s, 27H, H-$^tBu^{Pc}$), 1.69–1.74 (group s, 6H, 18^1-H^{pheo}, 8^2-H^{pheo}), from –0.95 to –2.35 (2 br, 2H,§ N-H^{pheo}). UV-Vis (toluene) λ nm (I/I_{max}): 352 (0.74), 415 (0.57), 509 (0.09), 538 (0.09), 618 (0.26), 647sh (0.28), 679 (1.00). UV-Vis (DMF) λ nm (I/I_{max}): 354 (0.58), 411 (0.45), 507 (0.04), 536 (0.04), 611 (0.19), 646sh (0.21), 676 (1.00). UV-Vis (THF) λ nm (I/I_{max}): 353 (0.66), 414 (0.65), 508 (0.10), 538 (0.10), 617 (0.26), 646sh (0.28), 678 (1.00). Fluorescence (toluene) λ nm (λ_{ex} = 610 nm): 686.

Preparation of micellar saline solutions based on dyad 3 and PVP (general procedure). A mixture of dyad **3** (*x* mmol) and PVP (*x*, 2*x* or 5*x* mmol) was dissolved in toluene to achieve homogeneity. The solvent was removed *in vacuo*, then 5 mL of saline solution were added to the resulting solid and the mixture was sonicated (16 W for *ca.* 1 min to transfer *ca.* 1 kJ of energy) until a homogeneous dispersion was obtained. The resulting dispersions (micellar solutions) were passed through the PTFE porous filters with 0.45 μm pore size to remove insoluble admixtures and microscale particles and used in DLS experiments without further treatment. Three solutions with different **3**÷PVP molar ratios were prepared.

*Micellar solution **3**÷**PVP (1:1)**.* A solution of dyad **3** (2.7 mg, 0.0019 mmol) and PVP (60 mg, 0.0015 mmol) in 5 mL of saline with C(**3**) = $3.7\cdot10^{-4}$ M and C(PVP) = $3\cdot10^{-4}$ M. This solution was additionally stored for 3 months in darkness at room temperature to give derivative solution **3**÷**PVP (1:1)t**.

*Micellar solution **3**÷**PVP (1:2)**.* A solution of dyad **3** (2.2 mg, 0.0015 mmol) and PVP (125 mg, 0.0031 mmol) in 5 mL of saline with C(**3**) = $3\cdot10^{-4}$ M and C(PVP) = $6.25\cdot10^{-4}$ M.

*Micellar solution **3**÷**PVP (1:5)**.* A solution of dyad **3** (2.8 mg, 0.0019 mmol) and PVP (396 mg, 0.0099 mmol) in 6.4 mL of saline with C(**3**) = $3\cdot10^{-4}$ M and C(PVP) = $15.46\cdot10^{-4}$ M.

Preparation of micellar solutions with working concentrations of **3** for DLS measurements was carried out by taking aliquots from the stock solution and adding them to 5 mL of water. The volume of aliquots and concentration of **3** in the resulting solutions (in parentheses) were as follows:

*For **3**÷**PVP (1:1)** and **3**÷**PVP (1:1)t***: 5 μL ($3.7\cdot10^{-7}$ M), 10 μL ($7.4\cdot10^{-7}$ M), 20 μL ($1.47\cdot10^{-6}$ M), 30 μL ($2.21\cdot10^{-6}$ M), 40 μL ($2.94\cdot10^{-6}$ M), 50 μL ($3.66\cdot10^{-6}$ M).

*For **3**÷**PVP (1:2)** and **3**÷**PVP (1:5)***: 5 μL ($3\cdot10^{-7}$ M), 10 μL ($6\cdot10^{-7}$ M), 20 μL ($1.2\cdot10^{-6}$ M), 30 μL ($1.8\cdot10^{-6}$ M), 40 μL ($2.4\cdot10^{-6}$ M), 50 μL ($3\cdot10^{-6}$ M).

The dependences of the R_h values on concentration of **3** in micellar solutions are shown in Figures 9–11.

Results and Discussion

The target dyad was obtained by transesterification reaction involving methylpheophorbide *a* (**1**) and functionally substituted zinc(II) phthalocyaninate **2** with terminal OH-group of benzyl type (Scheme 1) following the conditions recently developed in our group for the first synthesis of an analogous dyad composed of both metal-free phthalocyanine and methylpheophorbide *a* fragments.[32] As in the previous case, in order to exclude the oxidative processes during isolation of the target dyad **3**, we successfully utilized gel-permeation chromatography instead of the bulk sorption carriers (SiO_2, Al_2O_3). At the same time, a combination of gel-permeation chromatography and preparative TLC allowed to achieve a high-purity grade of the target compound.

The MALDI-TOF mass spectra of conjugate **3** and parent phthalocyanine **2** show intense molecular ion peaks (Figures 1 and S1, respectively, peak **I**) with isotopic patterns corresponding to theoretical ones (Figures 2 and S2, respectively). There are also peaks corresponding to the fragmentation of molecular ions at the ether bonds and, in the case of **3**, also at the ester bond of the spacer group. Thus, in the mass spectrum of **3**, there are two main phthalocyanine-derived peaks (Figure 1, peaks **II** and **III**) and one pheophorbide-derived peak (Figure 1, peak **IV**). Note that such fragmentation of $[M]^+$ *via* cleavage of the C–O bonds is characteristic for the phthalocyanines bearing peripheral phthalodiol groups.[23,24,42]

Compared to initial phthalocyanine **2**, target dyad **3** represents a mixture of both regioisomers and conformers, which should somewhat affect its NMR spectra. In such classical NMR solvents as $CDCl_3$, DMSO-d_6 and even DMF-d_7, the spectra of **3** reveal low resolution, *i.e.* the aggregation process takes place. Introduction of basic additives (Py-d_5, triethylamine) has practically no effect, while the tem-

‡ Precise integration is difficult due to overlap with water and solvent signals.

§ The observed integral value is lower due to H/D exchange interaction.

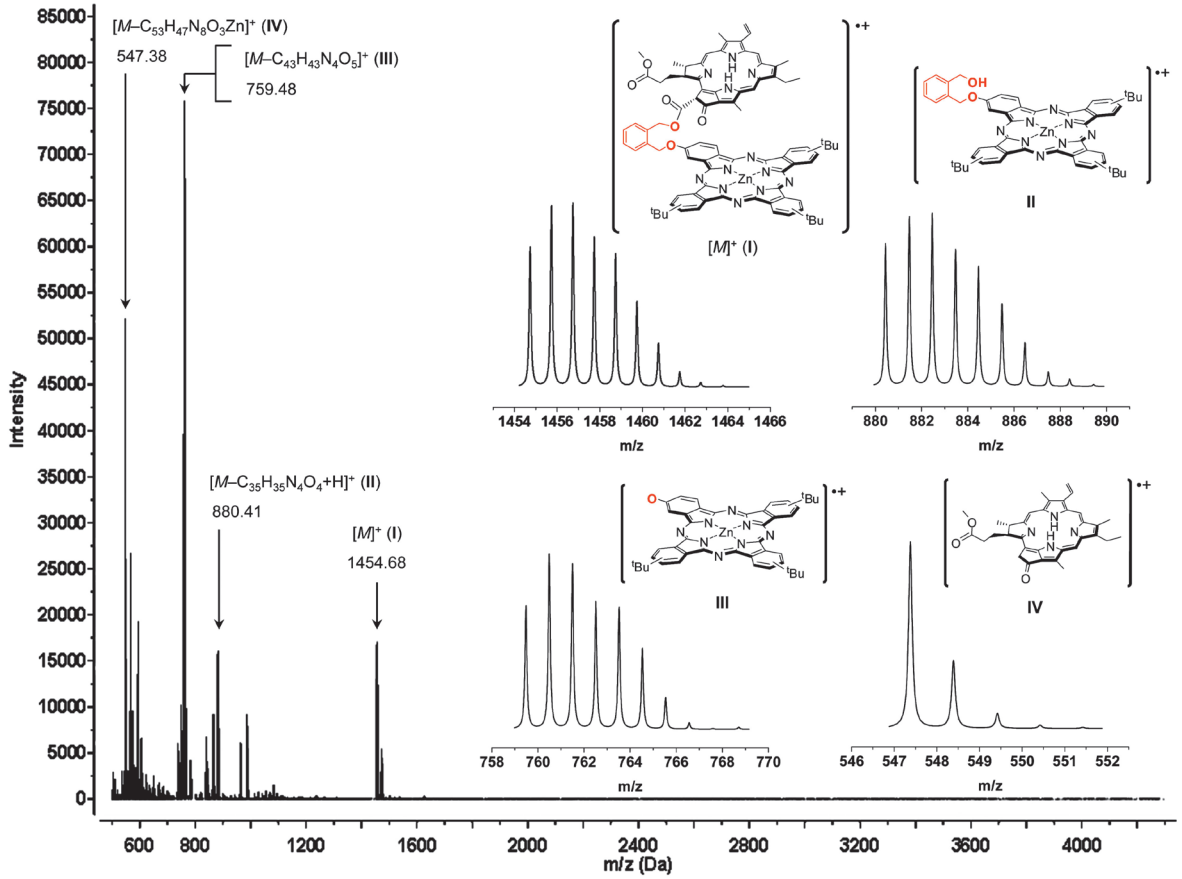

Figure 1. MALDI-TOF mass spectrum of dyad **3**. The inserts show isotopic distributions of $[M]^+$ (**I**) and some derivative ions (**II**–**IV**).

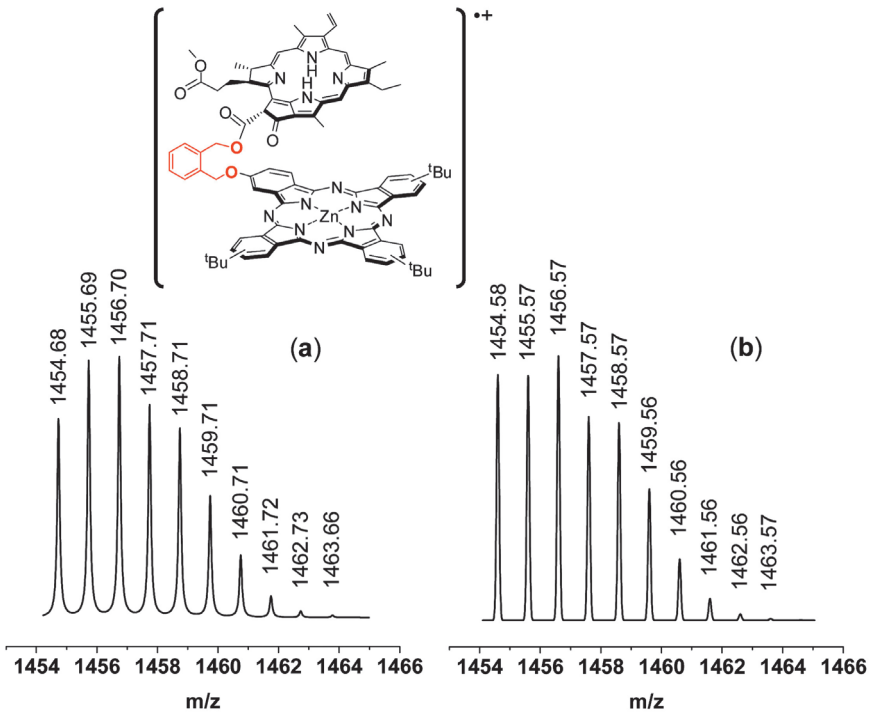

Figure 2. Isotopic distributions of $[M]^+$ of dyad **3**: (a) observed and (b) theoretical.

perature affects resolution the most. The observed solvent and temperature dependent changes in resolution imply that aggregation and conformational states determine the spectral line shape more than the presence of regioisomers. Figure 3 shows the ^{1}H NMR spectrum of **3** recorded in DMF-d_7 at 70 °C, which contains signals of phthalocyanine, pheophorbide and spacer moieties. For comparison, ^{1}H NMR spectra of initial compounds **1** and **2** are given in Figures S3 and S4, respectively. The assignment of signals in the ^{1}H spectrum of **3** was made on the basis of the corresponding data for **1**

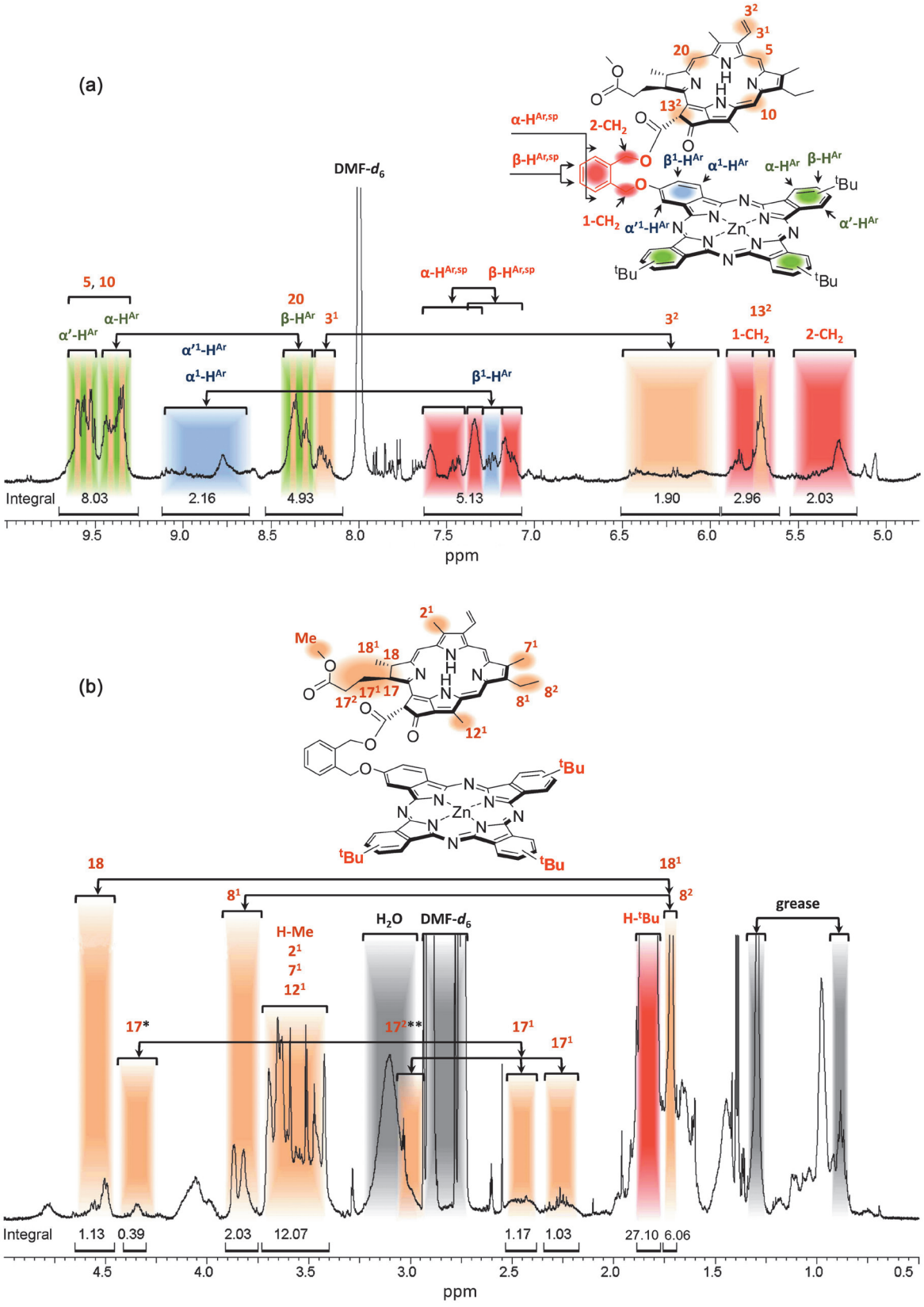

Figure 3. ^{1}H NMR spectrum of dyad **3** in DMF-d_7 at 70 °C: (a) aromatic and (b) aliphatic region. Areas assigned to the protons revealing spin-spin interactions according to the COSY data are connected by the arrows.

and **2** combined with the data obtained by the ^{1}H–^{1}H COSY technique (Figures S5 and S6). Based on this assignment, one should specially note that both upfield and downfield shifts are characteristic for different groups of protons in **3** compared to initial compounds **1** and **2** (Figure S7) indicating the presence of certain interactions between the constituting fragments. Thus, the highest values of upfield shifts ($\Delta\delta_u$, ppm) are characteristic for the region of the spacer group, in particular, for the protons α-H^{Ar,sp} ($\Delta\delta_u$ = 0.28), β-H^{Ar,sp} ($\Delta\delta_u$ = 0.24), β^1-H^{Ar} ($\Delta\delta_u$ = 0.28) and 13^2-H^{pheo} ($\Delta\delta_u$ = 0.56). In turn, the highest downfield shifts ($\Delta\delta_d$, ppm) were detected for the macrocyclic protons α-H^{Ar} ($\Delta\delta_d$ = 0.26) and α′-H^{Ar} ($\Delta\delta_d$ = 0.23), as well as for the protons of substituents 8^1-H^{pheo} ($\Delta\delta_d$ = 0.35), 3^1-H^{pheo} ($\Delta\delta_d$ = 0.36) and 17^2-H^{pheo} ($\Delta\delta_d$ = 0.41), which are relatively distant from the spacer. This qualitative assessment indicates that the strongest spatial interactions between the phthalocyanine, pheophorbide and spacer fragments in **3** are predictably observed in the area of the spacer group. At the same time, judging by the rather noticeable low-field shifts of some protons of the substituents, it can be concluded that parts of the molecule remote from the spacer can also take part in intramolecular inter-ligand interactions in solution.

For a deeper understanding of the structural features of conjugate **3**, we performed a DFT modeling with the determination of the most stable conformational states and some energy parameters. For comparative purposes, model systems based on starting compounds **1** and **2** were studied as well. The corresponding DFT-optimized structures **I**–**IV** are presented in Figure 4, and calculation parameters are given in Table 1.

During the PESs scan, two model structures of dyad **3** (**III** and **IV**) corresponding to local minima were found. For this purpose, two parameters were varied simultaneously – the angle of inclination of macrocycles (tilt angle) and the angle of their rotation in the ranges of 80–160° and 110–70°, respectively. The slope of the macrocycles was measured as the angle between the planes drawn through the intracyclic nitrogen atoms of both macrocycles; the rotation of macrocycles is responsible for the change in the angle between the vectors drawn in each macrocycle through the carbon atom adjacent to the spacer on each

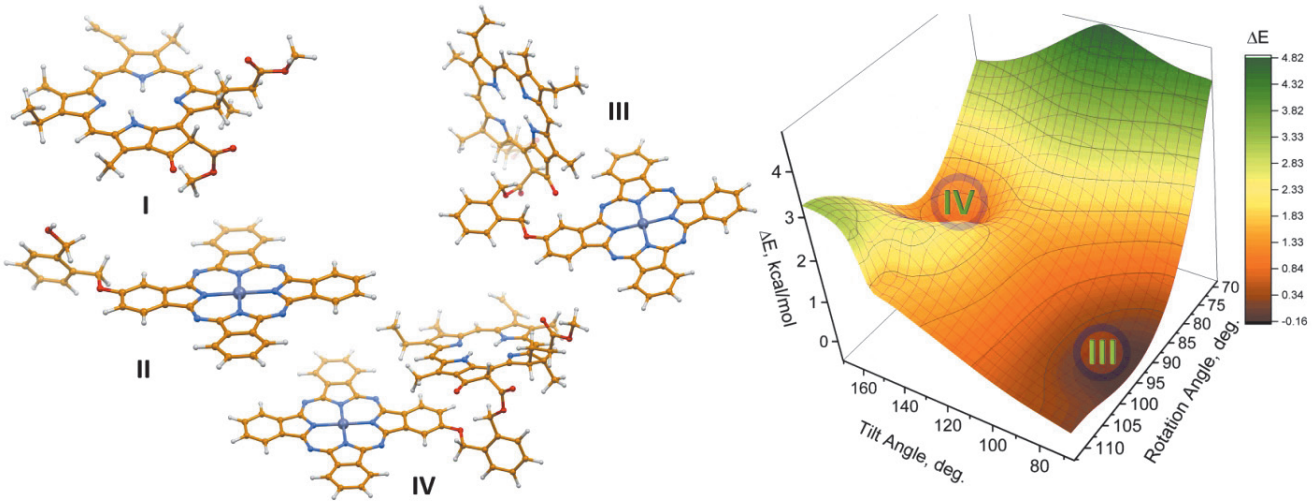

Figure 4. DFT-optimized structures of the models corresponded to the macrocyclic compounds (**I** and **II**) and the local minima (**III** and **IV**) on the PESs of tilting and rotating the macrocycles to find steady-state geometries.

Table 1. Selected calculation parameters of structures **I**–**IV** (B3LYP/6-31+G*).

Property	Structure			
	I	**II**	**III**	**IV**
Total Energy (*E*), a.u.	–1987.9800	–3904.4963	–5776.8600	–5776.8592
Bandgap (E_g),[a] eV	1.646	1.444	1.313	1.432
Dipole moment (μ), D	7.251	0.700	9.240	6.016
Polarizability (α), Å^3	33.28	46.75	79.58	71.65
First hyperpolarizability (β×10^{-30} esu)	18.64	13.55	18.70	21.86
Second hyperpolarizability (γ×10^{-34} esu)	1.04	–3.59	–2.71	1439.22

[a] $E_g = E_{LUMO} - E_{HOMO}$.

side, and the most distant carbon atom located in the plane of the same macrocycle. To build 3D surfaces, the so-called *kriging* was utilized. «Kriging» is the geostatistical method for interpolating related data. In our case, these are the angles of tilting and rotation of the macrocycles and the total energy of the system at a given moment. This method somewhat looks like the traditional least-squares method for some nonlinear functions. In contrast to the latter, it is implemented not in a plane, but space, and B-spline functions are used here as nonlinear functions. During interpolation, we did not use spline smoothing, because this will distort the heights and valleys on the 3D surface. We have implemented D. Krige's approach[51] numerically in the *Geometry Analyzer* Module for EasyQuanto.[49] As a result, a 50×50 matrix was obtained, based on which the 3D surface was built in the *Origin* 2015 program (Figure 4).

Structures **III** and **IV** differ in the arrangement of macrocycles and have an insignificant dissimilarity in energy – only 0.8 kcal/mol. Within structure **III**, macrocycles are twisted at about 90°, while in **IV** the angle between macrocycles is only 18°. The geometric features of both structures are due to the rigidity of the peripheral spacer. Macrocycles do not interact with each other and behave as individual subunits.

FF-DFT calculations show that the heterodimer may be of interest for a wide range of NLO applications. This is evidenced by the high dipole moments of the two most stable rotamers, acquired due to the pheophorbide unit. Rotamer, in which the macrocycles are located almost cofacial (*slipped-cofacial*, structure **IV**), demonstrates a high value of the second hyperpolarizability (γ), which is three orders of magnitude higher than the value for structures **I**–**III**. The *slipped-cofacial* rotamer may be of interest, in particular, for nonlinear light absorption, since γ is proportional to the two-photon absorption coefficient.[52] In addition, it is worth pointing out the negative sign of γ for the phthalocyanine unit and the angular conformer of the heterodimer. Organic materials with negative Re(γ) are self-defocusing and promising for optical switching and limiting applications.[38,53] Unlike structures **II** and **III**, pheophorbide **I** and *slipped-cofacial* rotamer **IV** can exhibit a self-focusing effect and may be of interest for strengthening input laser radiation.

The UV-Vis absorption spectrum of dyad **3** (Figure 5) exhibits panchromatic nature containing the bands of both pheophorbide and phthalocyanine counterparts and is practically close to a superposition of the spectra of initial compounds **1** and **2**. In order to investigate the possibility of Pheo-to-Pc intramolecular energy transfer in dyad **3**, which was previously discovered by the example of a similar dyad containing a free-base phthalocyanine,[32] as well as applied potential of **3** as an agent for theranostics, herein we investigated its fluorescent properties and the efficiency of singlet oxygen generation. Thus, when excited in the UV-Vis range, compound **3** shows red fluorescence with the spectral maximum at 686 nm (Figure 6). As the fluorescence maxima of compounds **1** and **2** are located at 676 and 684 nm, respectively, it can be stated that Pheo-to-Pc energy transfer indeed takes place in dyad **3**. The fluorescence quantum yields (Φ_f) in toluene solutions were determined to be: Φ_f(**1**) = 0.14; Φ_f(**2**) = 0.15; Φ_f(**3**) = 0.05. In turn, the singlet oxygen quantum yields (Φ_Δ) were measured as follows: Φ_Δ(**1**) = 0.65±0.05; Φ_Δ(**2**) = 0.68±0.05; Φ_Δ(**3**) = 0.54±0.05. Thus, the photophysical and photochemical parameters of conjugate **3** are of the same order that of its original components. Somewhat reduction of the Φ_f and Φ_Δ values for **3** compared to **1** and **2** can be provisionally explained by an increased decay of both singlet and triplet excited states by the internal conversion due to increased molecular size of the dyad and the presence of two interacting chromophores connected by a flexible linker. One can assume that upon interaction with biomolecules in living cells and tissues by adopting stable conformational states, the non-radiative relaxation of the excited states in **3** could be inhibited, and the efficiency of radiative processes, *i.e.* the Φ_f and Φ_Δ values, can be increased. This issue will become a subject for the further study.

For the successful practical implementation of a PS as a theranostic PDT agent, it is important to provide its targeted delivery to the cells of pathogenic tissues. One of the key principles of designing effective third-generation

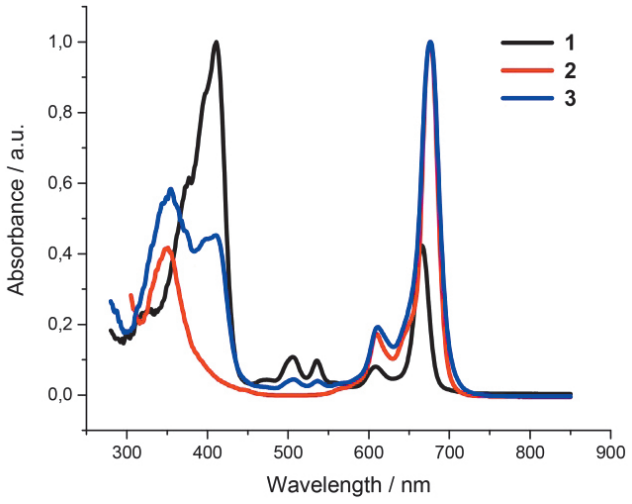

Figure 5. Normalized UV-Vis spectra of methylpheophorbide *a* (**1**), zinc phthalocyaninate **2** and dyad **3** in DMF.

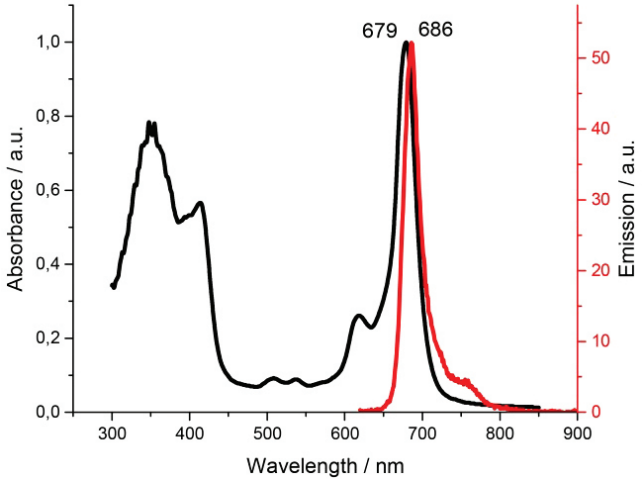

Figure 6. Normalized UV-Vis (black line) and fluorescence (red line) spectra of dyad **3** in toluene.

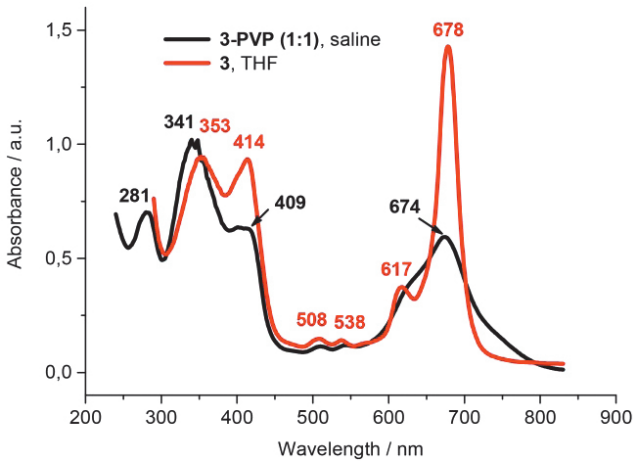

Figure 7. UV-Vis spectra of micellar solution **3÷PVP (1:1)** in saline (black line) and **3** in THF (red line). Concentration of **3** equals *ca.* $3 \cdot 10^{-5}$ M in both solutions.

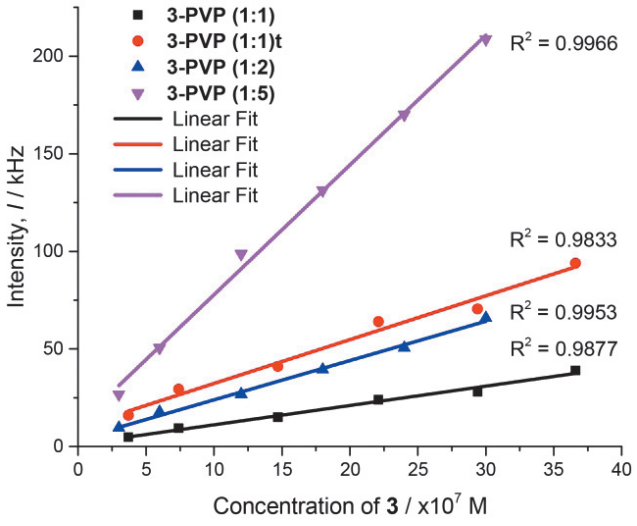

Figure 8. Concentration dependences of scattered light intensity (*I*) for micellar solutions **3÷PVP (1:1)**, **3÷PVP (1:1)t**, **3÷PVP (1:2)** and **3÷PVP (1:5)** with the corresponding linear fits and coefficient of determination (R^2) values.

PSs is the use of nanoscale liposomal or micellar containers, which not only ensure the PS's solubility in aqueous media, particularly at physiological pH, and contribute to its safe transportation through the bloodstream, but also significantly increase the selectivity of its delivery and accumulation in tumor tissues due to their characteristic enhanced permeability and retention (EPR) effect.[54 and ref. therein] This effect represents one of the «passive targeting» mechanisms and is observed for particles ranging in size from 20 to 200 nm with an optimum of about 100 nm. Note that the lower limit is determined by the functional permeability of healthy tissues, which is about 7 nm, while as size increases beyond 150 nm, more and more nanoparticles are entrapped within the liver and spleen.

In this work, we prepared three micellar solutions based on dyad **3** and PVP as solubilizing biocompatible polymer with the molar ratios of 1:1, 1:2 and 1:5, respectively, and studied the size evolution patterns of the formed nanoparticles depending on the ratio of components, concentration and storage time by the DLS technique.

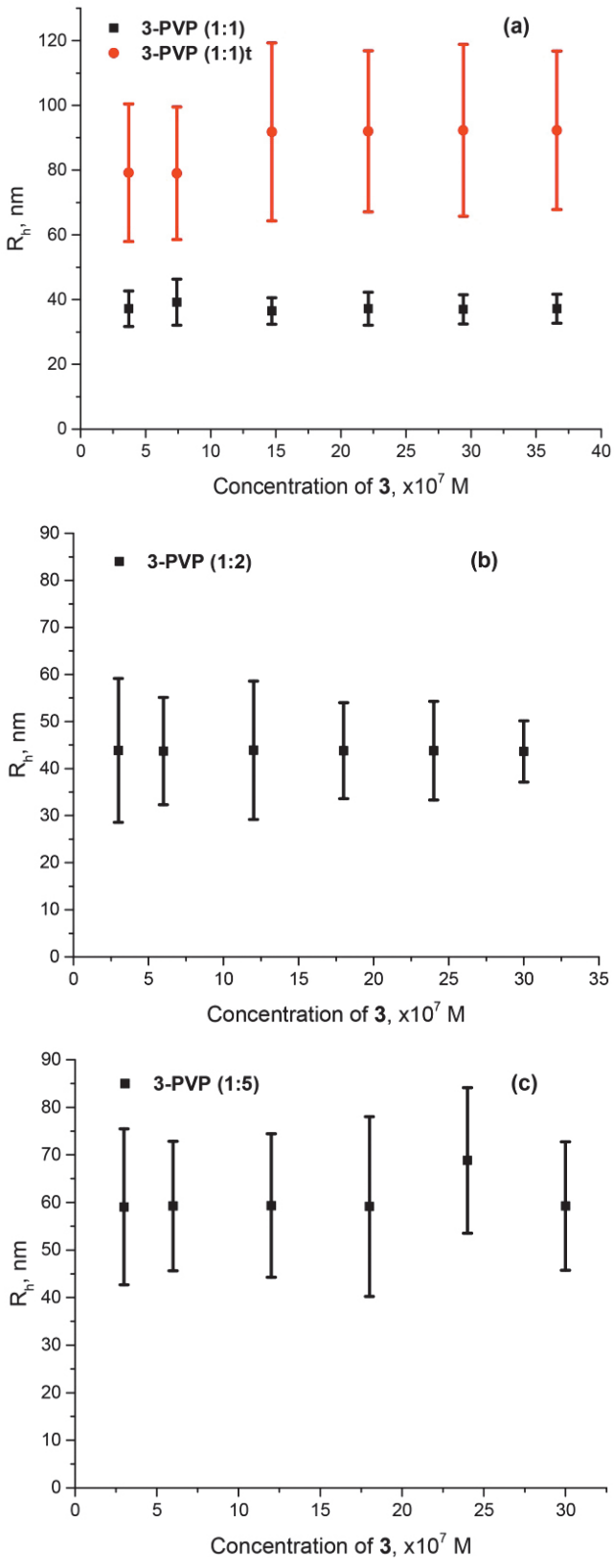

Figure 9. Concentration dependences of hydrodynamic radii (R_h) values for micellar solutions: (a) **3÷PVP (1:1)** and **3÷PVP (1:1)t**, (b) **3÷PVP (1:2)** and (c) **3÷PVP (1:5)**. Corresponding error values are shown by the bars.

A typical UV-Vis spectrum of the resulting micellar solutions illustrated by the example of **3÷PVP (1:1)** is shown in Figure 7 and indicates some aggregation of dyad **3** molecules. At the same time, we can state that there is a high solubilizing effect of PVP in this system, which is actually a water-based solution of hydrophobic compound **3**.

The dependences of the scattered light intensity (*I*) on the concentration for **3÷PVP** solutions (Figure 8) are linear with high R^2 values, which indicates the absence of significant effects of laser radiation on the structure of the studied nanoparticles with a total exposure time of more than 50 min for each sample. The hydrodynamic radii (R_h) values do not show significant concentration dependences (Figure 9), which indicates the stability of the resulting micelles in a given concentration range. In turn, an increase in the PVP molar percentage leads to a gradual increase in the size of nanoparticles, which was recently demonstrated for derivatives of the same structural type.[55] Thus, with an increase in **3**÷PVP ratio from 1:1 to 1:5 (Table 2), an almost 2-fold increase in the R_h values is observed. In addition, during the long-term storage of sample **3÷PVP (1:1)**, there was an almost 3-fold increase in the particle size to values of the order of 90 nm (sample **3÷PVP (1:1)t**, Figure 9a, Table 2). Thus, the R_h values measured for **3÷PVP** micellar solutions are close to optimal for the implementation of the EPR effect, which makes them promising PS systems in the «passive targeting» concept.

Table 2. Selected DLS measurement parameters of **3÷PVP** micellar solutions.

Sample	*C*(**3**), μM	*I*, kHz	R_h, nm
3÷PVP (1:1)	3.66	39	37.2±4.7
3÷PVP (1:2)	3	65.9	43.6±6.5
3÷PVP (1:5)	3	208.7	59.3±15.2
3÷PVP (1:1)t	3.66	94	92.1±24.8

Conclusions

In summary, we first synthesized covalent metal phthalocyaninate–methylpheophorbide *a* dyad **3** following a simple and effective transesterification of α-keto methyl ester group of methylpheophorbide *a*. In the MALDI-TOF mass-spectrum of **3**, along with the intense molecular ion peak, several phthalocyanine- and pheophorbide-derived fragmentation peaks are observed responsible for cleavage of the C–O bonds of the spacer, which is typical for tetrapyrroles bearing peripheral phthalodiol groups. The ^{1}H NMR data supported by theoretical studies evidence on somewhat steric bulkiness of **3**, which results in certain intramolecular interactions. Thus, the performed DFT calculations allowed determination of two stable conformational states in the model structure of **3** both having high dipole moment and polarizability values. Moreover, one of the rotamers shows a second hyperpolarizability value three orders of magnitude higher than the corresponding values for the models of initial compounds. This suggests a high applied potential of dyad **3** as a nonlinear light absorbing material. The UV-Vis absorption spectrum of **3** shows the bands of both the phthalocyanine and pheophorbide subunits revealing its panchromatic nature, while the fluorescence maximum of **3** at 686 nm is close to the one of the initial zinc phthalocyaninate indicating the implementation of the FRET process. In addition, **3** effectively generates singlet oxygen, and the prepared **3÷PVP** compositions are perfectly soluble in saline forming stable micelles ranging between 40 and 100 nm in diameter. These parameters perfectly fit the EPR nanodelivery conditions rendering **3÷PVP** nanoparticles as perspective PSs for PDT/imaging theranostic purposes.

Acknowledgements. We thank Dr. Olga A. Maloshitskaya for recording the MALDI-TOF spectra and Dr. Alexander V. Chernyak and Vladimir I. Shestov for recording the NMR spectra. NMR experiments have been performed using the equipment of the Multi-User Analytical Center of IPCP RAS and the facilities provided by the Center of Collective Use of IPAC RAS. Theoretical studies were supported by Russian Science Foundation Grant 21-73-20016. Synthetic and spectral studies were performed within the framework of the State Assignment of 2021 (Theme 45.5 Creation of compounds with given physicochemical properties, No. 0090-2019-0003). The authors also thank the Joint Supercomputer Center of RAS (*www.jscc.ru*) for providing computing resources.

References

1. Lo P.-C., Leng X., Ng D.K.P. *Coord. Chem. Rev.* **2007**, *251*, 2334–2353.
2. Pereira A.M.V.M., Soares A.R.M., Hausmann A., Neves M.G.P.M.S., Tome A.C., Silva A.M.S., Cavaleiro J.A.S., Guldi D.M., Torres T. *Phys. Chem. Chem. Phys.* **2011**, *13*, 11858–11863.
3. Kandhadi J., Kanaparthi R.K., Giribabu L. *J. Porphyrins Phthalocyanines* **2012**, *16*, 282–289.
4. Yamada Y., Mihara N., Tanaka K. *Dalton Trans.* **2013**, *42*, 15873–15876.
5. Maligaspe E., Kumpulainen T., Lemmetyinen H., Tkachenko N.V., Subbaiyan N.K., Zandler M.E., D'Souza F. *J. Phys. Chem. A* **2010**, *114*, 268–277.
6. Jacobs R., Stranius K., Maligaspe E., Lemmetyinen H., Tkachenko N.V., Zandler M.E., D'Souza F. *Inorg. Chem.* **2012**, *51*, 3656–3665.
7. KC C.B., Ohkubo K., Karr P.A., Fukuzumi S., D'Souza F. *Chem. Commun.* **2013**, *49*, 7614–7616.
8. KC C.B., Lim G.N., Karr P.A., D'Souza F. *Chem. Eur. J.* **2014**, *20*, 7725–7735.
9. KC C.B., Lim G.N., D'Souza F. *Nanoscale* **2015**, *7*, 6813–6826.
10. Zhang Y., Xue Z., Qi D., Wang K., Liu H., Jiang J. *Chem. Eur. J.* **2017**, *23*, 15017–15021.
11. Zhang D., Zhu M., Zhao L., Zhang J., Wang K., Qi D., Zhou Y., Bian Y., Jiang J. *Inorg. Chem.* **2017**, *56*, 14533–14539.
12. Qi D., Zhang J., Zhang D., Zhu M., Gong L., Su C., Lu W., Bian Y., Jiang J. *Dyes Pigm.* **2020**, *173*, 107941.
13. Liu W., Wang K., Wang C., Liu W., Pan H., Xiang Y., Qi D., Jiang J. *J. Mater. Chem. A* **2018**, *6*, 22851–22857.
14. Kameyama K., Satake A., Kobuke Y. *Tetrahedron Lett.* **2004**, *45*, 7617–7620.
15. Feng X., Ding X., Chen L., Wu Y., Liu L., Addicoat M., Irle S., Dong Y., Jiang D. *Sci. Rep.* **2016**, *6*, 32944.

16. KC C.B., Stranius K., D'Souza P., Subbaiyan N.K., Lemmetyinen H., Tkachenko N.V., D'Souza F. *J. Phys. Chem. C* **2013**, *117*, 763–773.
17. Wang X., Hu J., Wang P., Zhang S., Liu Y., Xiong W., Liu Q. *Theranostics* **2015**, *5*, 772–786.
18. Martinez De Pinillos Bayona A., Mroz P., Thunshelle C., Hamblin M.R. *Chem. Biol. Drug. Des.* **2017**, *89*, 192–206.
19. Josefsen L.B., Boyle R.W. *Theranostics* **2012**, *2*, 916–966.
20. Krasia-Christoforou T., Georgiou T.K. *J. Mater. Chem. B* **2013**, *1*, 3002–3025.
21. Zhao L., Kim T.-H., Ahn J.-C., Kim H.-W., Kim S.Y. *J. Mater. Chem. B* **2013**, *1*, 5806–5817.
22. Ryan A.A., Senge M.O. *Photochem. Photobiol. Sci.* **2015**, *14*, 638–660.
23. Tolbin A.Yu., Pushkarev V.E., Tomilova L.G. *Mendeleev Commun.* **2009**, *19*, 78–80.
24. Tolbin A.Yu., Pushkarev V.E., Nikitin G.F., Tomilova L.G. *Tetrahedron Lett.* **2009**, *50*, 4848–4850.
25. Pushkarev V.E., Tolbin A.Yu., Borisova N.E., Trashin S.A., Tomilova L.G. *Eur. J. Inorg. Chem.* **2010**, 5254–5262.
26. Pushkarev V.E., Tolbin A.Yu., Zhurkin F.E., Borisova N.E., Trashin S.A., Tomilova L.G., Zefirov N.S. *Chem. Eur. J.* **2012**, *18*, 9046–9055.
27. Tolbin A.Yu., Pushkarev V.E., Shulishov E.V., Tomilova L.G. *J. Porphyrins Phthalocyanines* **2012**, *16*, 341–350.
28. Tolbin A.Yu., Pushkarev V.E., Balashova I.O., Brel V.K., Gudkova Yu.I., Shestov V.I., Tomilova L.G. *J. Porphyrins Phthalocyanines* **2013**, *17*, 343–350.
29. Tolbin A.Yu., Pushkarev V.E., Balashova I.O., Tomilova L.G. *Mendeleev Commun.* **2013**, *23*, 137–139.
30. Tolbin A.Yu., Pushkarev V.E., Balashova I.O., Dzuban A.V., Tarakanov P.A., Trashin S.A., Tomilova L.G., Zefirov N.S. *New J. Chem.* **2014**, *38*, 5825–5831.
31. Tolbin A.Yu., Pushkarev V.E., Sheinin V.B., Shabunin S.A., Tomilova L.G. *J. Porphyrins Phthalocyanines* **2014**, *18*, 155–161.
32. Balashova I.O., Pushkarev V.E., Shestov V.I., Tomilova L.G., Koifman O.I., Ponomarev G.V. *Macroheterocycles* **2015**, *8*, 233–238.
33. Tolbin A.Yu., Pushkarev V.E., Tomilova L.G., Zefirov N.S. *J. Porphyrins Phthalocyanines* **2017**, *21*, 128–134.
34. Tolbin A.Yu., Pushkarev V.E., Sedova M.V., Maklakov S.S., Tomilova L.G. *Spectrochim. Acta A: Mol. Biomol. Spectrosc.* **2018**, *205*, 335–340.
35. Korostei Yu.S., Tolbin A.Yu., Dzuban A.V., Pushkarev V.E., Sedova M.V., Maklakov S.S., Tomilova L.G. *Dyes Pigm.* **2018**, *149*, 201–211.
36. Korostei Yu.S., Tarasova V.G., Pushkarev V.E., Borisova N.E., Vorobiev A.Kh., Tomilova L.G. *Dyes Pigm.* **2018**, *159*, 573–575.
37. Korostei Yu.S., Pushkarev V.E., Tolbin A.Yu., Dzuban A.V., Chernyak A.V., Konev D.V., Medvedeva T.O., Talantsev A.D., Sanina N.A., Tomilova L.G. *Dyes Pigm.* **2019**, *170*, 107648.
38. Tolbin A.Yu., Brel V.K., Tarasevich B.N., Pushkarev V.E. *Dyes Pigm.* **2020**, *174*, 108095.
39. Patent RF 2276976, **2006**.
40. Patent RF 2330037, **2008**.
41. Patent RF 2490273, **2013**.
42. Tolbin A.Yu., Tomilova L.G., Zefirov N.S. *Russ. Chem. Bull., Int. Ed.* **2005**, *54*, 2099–2103.
43. Seybold P.G., Gouterman M., Callis J. *Photochem. Photobiol.* **1969**, *9*, 229–242.
44. Fery-Forgues S., Lavabre D. *J. Chem. Educ.* **1999**, *76*, 1260–1264.
45. Zenkevich E., Sagun E., Knyukshto V., Shulga A., Mironov A., Efremova O., Bonnett R., Songca S.P., Kassem M. *J. Photochem. Photobiol. B: Biol.* **1996**, *33*, 171–180.
46. Laikov D.N. *Chem. Phys. Lett.* **1997**, *281*, 151–156.
47. Ernzerhof M., Scuseria G.E. *J. Chem. Phys.* **1999**, *110*, 5029–5036.
48. Laikov D.N. *Chem. Phys. Lett.* **2005**, *416*, 116–120.
49. Tolbin A.Yu. The control system of the quantum-chemical calculations – EasyQuanto. Certificate of state registration of computer program 2015619026 (RU), **2015**.
50. Schmidt M.W., Baldridge K.K., Boatz J.A., Elbert S.T., Gordon M.S., Jensen J.H., Koseki S., Matsunaga N., Nguyen K.A., Su S., Windus T.L., Dupuis M., Montgomery Jr. J.A. *J. Comput. Chem.* **1993**, *14*, 1347–1363.
51. Bayraktar H., Turalioglu F.S. *Stoch. Environ. Res. Risk Assess.* **2005**, *19*, 301–305.
52. Ngoy B.P., May A.K., Mack J., Nyokong T. *J. Mol. Struct.* **2019**, *1175*, 745–753.
53. Gieseking R.L.M. *Chem. Mater.* **2019**, *31*, 6850–6859.
54. Blanco E., Shen H., Ferrari M. *Nat. Biotechnol.* **2015**, *33*, 941–951.
55. Krot A.R., Stroganova J.D., Sergeeva I.A., Fedorova K.V., Korostey J.S., Balashova I.O., Pushkarev V.E., Tarakanov P.A. *Memoirs of the Faculty of Physics* **2018**, *3*, 1830702.

Received 23.03.2021
Accepted 14.04.2021